Procedia Computer Science

Volume 80, 2016, Pages 999–1010

ICCS 2016. The International Conference on Computational Science

Supermodeling in simulation of melanoma progression

W. Dzwinel[1], A. Kłusek[1] and O.V.Vasilyev[2]

[1]*AGH University of Science and Technology, Department of Computer Science, Krakow, Poland*
[2]*University of Colorado at Boulder, Department of Mechanical Engineering, Boulder, USA*
dzwinel@agh.edu.pl, klusek@student.agh.edu.pl, oleg.vasilyev@colorado.edu

Abstract

Supermodeling is an interesting and non-standard concept used recently for simulation of complex and non-linear systems such as climate and weather dynamics. It consists in coupling of a few "imperfect" sub-models to create the "superior" supermodel. We discuss here the supermodeling strategy in the context of tumor growth simulation. To check its adaptive flexibility we have developed a basic, but still computationally complex, 3-D modeling framework of melanoma growth. The supermodel of melanoma consists of a few coupled sub-models, which differ in values of a parameter responsible for tumor cells and extracellular matrix interactions. We demonstrate that due to synchronization of sub-models, the supermodel is able to simulate qualitatively different scenarios of cancer growth than those observed for sub-models when run separately. These scenarios correspond to the basic types of melanoma cancer. This property makes the supermodel very flexible to follow and to predict real cases of melanoma development through learning the coupling coefficients between sub-models from real data. On the basis of preliminary simulation results, we discuss the prospects of supermodeling strategy as a promising coupling factor between formal and data-based models of tumor.

Keywords: supermodeling, melanoma growth, computer simulation

Introduction

Mathematical and computer modeling of cancer is one of the greatest challenge in computational biology and the principal goal of computational oncology. There are numerous overview papers and books about modeling of tumor dynamics, which contain the knowledge and experience collected during almost 40 years of history of cancer simulation (see, e.g., Bellomo, et al., 2008; Vittorio and Lowengrub, 2010; Deisboeck and Stamatakos 2010; Deisboeck, et al., 2011; Barillot, et al., 2012; Wolkenhauer, et al., 2014, Wodarz and Komarova, 2014). Though the progress in deeper conceptual understanding of interactions between multiple multiscale processes taking part in the cancerogenesis cannot be underestimated, the habitual application of cancer progression monitoring in clinical medicine by employing computer simulations is still in an infant stage. Countless of interrelated microscopic and macroscopic factors underlying tumor development from the moment of its birth to

Selection and peer-review under responsibility of the Scientific Programme Committee of ICCS 2016

doi:10.1016/j.procs.2016.05.396

its irresistible proliferation throughout the whole organism, highly complicated growth medium, very individual properties of invaded organism and its surrounding environment, and sensibility on current physical conditions, make the whole system computationally irreducible. Therefore, making longer and reliable prognosis about tumor dynamics just on the basis of mathematical models (even well parametrized) and assumed initial conditions (even well defined) is a nonsense like that of weather forecast for a week by using only existing numerical models and current measurements of temperature, pressure, humidity and wind fields. The intuitive approach to make computer simulation useful for predicting dynamics of such the complex systems is prediction/correction scheme, where numerical simulations are continually verified by incoming data and are reinforced by data models. In our opinion, data-based models will be in the future the key modeling components in predicting behavior of biological systems. The formal mathematical models could play the role of an additional knowledge, which defines more precisely the feature space topology for machine learning tools. In this context, the following question can be posed: How complex and detailed such the models should be?

In machine learning, very complicated data models involving many parameters are difficult to teach (adapt to data) and are prone to overfitting. Hence, their usefulness in generalization and knowledge extraction can be questionable. Exactly the same deficiency concern intricate mathematical models, which – taking into account their nonlinearity – may become completely out of control, producing numerical and methodological artifacts. The state of the art in machine learning shows that ensemble learning, where data models are made of coupled simple sub-models, results in the best classifiers. It can be observed following the successes of boosting algorithms, neural networks (Alpaydin, 2014) and recently the Hinton's deep belief networks (Hinton et al., 2006). Such the ensemble models are adapted to data through learning both the parameters of sub-models and their coupling strength.

Very similar concept can be applied when imperfect or approximate formal models of a complex process are available. In this case, the supermodel is created as a combination of coupled sub-models (van den Berge, et al., 2011). However, unlike in ensemble learning, only the coupling coefficients between sub-models can be learned from data. The imprecise fit of their internal parameters can be compensated assuming that they values are different in every sub-model. The role of coupling coefficients is to correct sub-models imperfections and fit them to real data via synchronization. Synchronization is the fundamental phenomenon, which allows for coordinating the dynamics of multiple mutually coupled systems. In (Duane, et al., 2006; Yang, et al., 2006) the synchronization mechanism was proposed as a method for data assimilation in climate science. Moreover, it was shown in (Duane, 2009) that by coupling various imprecise models and by developing a supermodel, one can increase substantially modeling quality and efficiency. The research teams from SUMO FET European Project (http://projects.knmi.nl/sumo/) greatly extended the theory and practice of supermodeling. They employ synchronization mechanism to construct ensembles of coupled models consisting of perturbed variants of a single model, heterogeneous models and ensembles of heterogeneous models (e.g. atmosphere and ocean models). It was shown that by assuming sufficient coupling strength, the sub-models in the supermodel can synchronize and come into a consensus state. Furthermore, when coupling coefficients are learned from data, the dynamics of the synchronized state may provide a better representation of realistic behavior than the sub-models would do.

In this paper we propose to apply the supermodeling strategy for simulating cancer proliferation. To this end we have developed a computational model of melanoma skin cancer. It is based on a single phase continuum mathematical description and includes only the most important tumor growth factors such as angiogenesis, vascular system remodeling, and basic interactions of tumor cells with extracellular matrix. The mathematical model of cancer and its parameters were taken from the previously published papers (Chaplain, et al., 2006; Welter and Rieger, 2010). We have embedded it in the layout mimicking realistic skin structure. To simulate tumors of one centimeter in size or larger, in a reasonable computational time, we have implemented our model in CUDA GPU environment. Moreover, in contrast to the previous models (Chaplain, et al., 2006; Welter and Rieger, 2010), we

have added additional terms responsible for interaction between cancer cells and extracellular matrix (Ramis-Conde, et al., 2008). Tumor growth speed is monotonically dependent on a constant, which parametrizes this term. The supermodel of melanoma consists of coupled "imperfect" models differing in the values of this parameter.

In the case of weather dynamics, the trajectories are located on a strange attractor of a finite volume in the phase space. Meanwhile, the type of initial conditions of tumor growth is very different, what may considerably influence sub-models synchronization. Therefore, we address here the question if the competitive growth simulated by tumor sub-models will not hamper the synchronization between them. In the following sections we present the main principles of supermodeling, the computational model of melanoma, and simulation results of melanoma supermodeling. Finally, we discuss the conclusions and the main directions of future work.

Supermodeling principles

Here we describe briefly the supermodeling basics with original notation from (van den Berge, et al., 2011). Let us assume that the supermodel consists of a few μ=1,...,M imperfect sub-models, which are described by a set of differential equations (ODE or PDE) of the form:

$$\dot{x}_\mu^i = f_\mu^i(x_\mu, t) \tag{1}$$

where the state vector $\mathbf{x}_\mu = (x_\mu^1, ..., x_\mu^m)$ consists of m dynamical system variables. We introduce coupling terms between sub-models μ and ν such as:

$$\dot{x}_\mu^i = f_\mu^i(x_\mu, t) + \sum_\nu C_{\mu\nu} \cdot \left(x_\mu^i - x_\nu^i\right) \tag{2}$$

where coupling tensor $\mathbf{C} = \{C_{\mu\nu}^i\}$. The supermodel evolution $\mathbf{x}_{\text{sumo}}$ with time t is described by the ensemble average, i.e.:

$$x_{sumo}(C, t) \equiv \frac{1}{M} \cdot \sum_\mu x_\mu(C, t) \tag{3}$$

.

A measure of the quality of synchronization between μ and ν is the average of squared distance between corresponding points. The synchronization error is defined as follows:

$$e^i(t) = \frac{1}{lp} \sum_{(\mu,\nu)} \frac{1}{N} \sum_{k=0}^{N-1} \left[x_\mu^i(k\Delta\mathbf{r}, t) - x_\nu^i(k\Delta\mathbf{r}, t) \right] \tag{4}$$

where: N is the number of computational grid nodes, lp is the number of (μ, ν) pairs, $\Delta\mathbf{r}$ is the grid vector. The tensor of coupling coefficients $\mathbf{C}=\{\mathbf{C}_{\mu\nu}^i\}$ is learned from the "ground truth" (data) vector $\mathbf{x}_{\text{gt}}$ by minimizing the weighed squared error $E(\mathbf{C})$ in K following timesteps, i.e.:

$$E(C) = \frac{1}{k\Delta} \sum_{i=1}^{K} \int_{t_i}^{t_i+\Delta} \left| \mathbf{x}_{sumo}(C, t) - \mathbf{x}_{gt}(t) \right|^2 \tag{5}$$

where γ^t is a discount factor, with $0<\gamma< 1$ (van den Berge, et al., 2011). The error function $E(\mathbf{C})$ measures a supermodel error and internal error (numerical error, imperfection of initial conditions etc.) growth. The second term surpasses the first one at later times in the short-term integration (see (van den Berge, et al., 2011)). The discount factor is included to decrease the contribution of internal error increase.

There are many questions which have to be answered prior the supermodel development: How to combine the individual models? By coupling of all or only some of the most important dynamical variables? Or maybe by exchanging some fields or fluxes as it is in climate modeling (Hiemstra, et al., 2012; Mirchev, et al., 2012)?. Can the supermodel follow changes in the real system, which are unknown for sub-models but are present in training data? In this context the remarkable result was published in (van den Berge, et al., 2011). It was shown that the supermodel made of imperfect Lorenz

systems was able to accurately follow the modifications of the Lorenz attractor. Another problem with supermodeling is that there are many local minimums of $E(\mathbf{C})$. As shown in (Hiemstra, et al., 2012), with different starting conditions completely different values of C can be found. It appeared, however, that the supermodels with these various minimums all produce very similar attractors close to the "ground truth" with about the same performance quality.

As shown in (van den Berge, et al., 2011; Hiemstra, et al., 2012), not all dynamical system variables have to be coupled. Particularly, in case of some complexity constrains. Similarly, when the sub-models are incomplete and are focused on different aspects of reality, some dynamical variables cannot be shared by all of them. This is the reason to consider partially coupled sub-model ensemble as well.

The supermodeling is a very interesting idea, which is used for climate and weather simulation. However, unlike climate and weather, many complex biological phenomena – such as tumor proliferation – represent growth dynamics. In this case, subsequent patterns produced by the system in time are substantially different from those obtained in the past and in the future. Additionally, they strongly depend on a growth setup and initial simulation conditions. Therefore, the question can be addressed here if the supermodeling can also be used for modeling the systems representing growth dynamics?

Melanoma supermodel

Melanoma belongs to the most aggressive and malignant tumors. This neoplasm has the highest resistance to anticancer therapy in its advanced stage (seer.cancer.gov/statfacts/html/melan.html). Up to now, to the best of our knowledge, there are no computer models of melanoma dynamics in an environment simulating skin. To this end, we have developed a general model of melanoma on the basis of models published in (Chaplain, et al., 2006; Ramis-Conde, et al., 2008; Welter and Rieger, 2010; Manning, 2013) and we have created a setup that mimics layers and vasculature of real skin (see Fig.1).

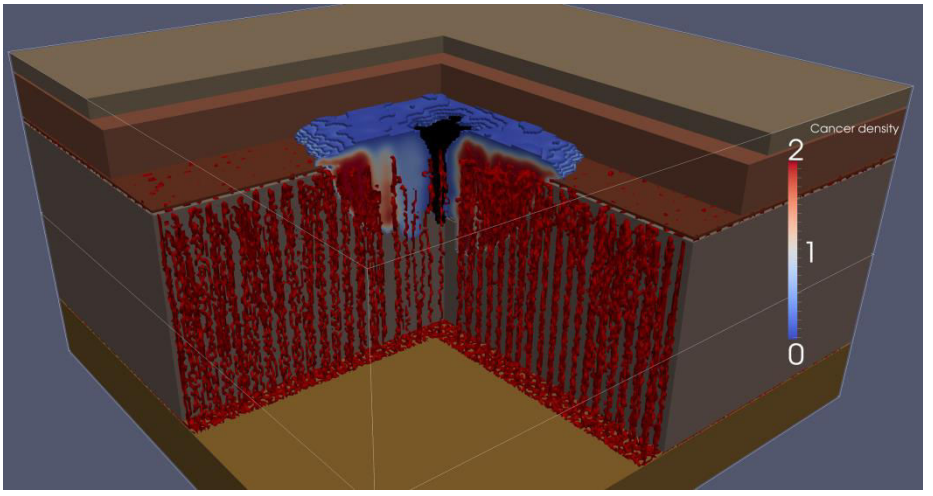

Figure 1: The modeling layout with growing melanoma at the center. The skin tissue layers are depicted from the top to the bottom as follows: *stratum corneum, stratum spinosum, basement membrane, dermis and hypodermis*. The vasculature is shown in red and the tumor from black (the necrotic center) through blue (the lowest concentration of cancer cells) to red (the highest concentration of cancer cells).

Of course, the skin vasculature is greatly simplified comparing to the real one. It is modeled by two regular meshes of blood capillaries placed horizontally on the top of *dermis* and *hypodermis*, respectively. Their nodes are connected by vertical blood vessels. The Dirichlet boundary conditions are defined at the computational box boundaries. The tumor starts to growth at the center of the *epidermis* just above the *basement membrane*. Our mathematical model of melanoma is of a single phase continuous type (Vittorio and Lowengrub, 2010). It is described by means of mainly diffusion-reaction partial differential equations. Their numerical integration simulate spatio-temporal evolution of density fields of tumor angiogenic factors (TAF), oxygen, cancer cells and the process of vascular remodeling. Below we enumerate the main equations describing the tumor model, which come mainly from (Chaplain, et al., 2006; Welter and Rieger, 2010). The parameters description and their values, adopted from (Ramis-Conde, et al., 2008; Chaplain, et al., 2006; Welter and Rieger, 2010; Barillot, et al., 2012; Manning, 2013), are collected in Table 1.

a) The equation below describes endothelial cell dynamics, i.e., the vascular network evolution. We denote by n the endothelial cell density per unit area, which spatio-temporal evolution is as follows:

$$\frac{\partial n}{\partial t} = D_n \Delta n - \nabla \cdot (X(c) \nabla c n) - \rho_n \cdot (n \nabla f) \tag{6}$$

b) The chemotactic migration is characterized by the $X(c)$ function, which reflects the decrease in chemotactic sensitivity with increased TAF concentration and:

$$X(c) = \frac{\chi_n}{1 + \delta_n c} \tag{7}$$

c) Tumor angiogenic factors (TAF) concentration c decays close to blood vessels according to:

$$\frac{\partial c}{\partial t} = -\eta_c \eta_i c \tag{8}$$

where n_i=1 in the vicinity of endothelial cells and 0 elsewhere.

d) The following equation describes the spatio-temporal changes in fibronectin concentration, i.e.,

$$\frac{\partial f}{\partial t} = \beta_f n_i - \gamma_f m f \tag{9}$$

e) The equation below represents the evolution of density field of Matrix Degrading Enzymes (MDE). Proliferating endothelial cells secrete MDE to penetrate the extracellular matrix (ECM).

$$\frac{\partial m}{\partial t} = \alpha_m n_i + \varepsilon_m \Delta m - \nu_m m \tag{10}$$

f) The oxygen concentration is described by the Poisson equation, where $o^{(B)}$ is the blood O_2 level:

$$\Delta o - \gamma_o o + \alpha_o \left(o^{(B)} - o \right) = 0 \tag{11}$$

g) Hypoxic tumor cells (which means that locally $o<o_{TC}$) produce TAF. Its concentration c in the tissue is computed by using Greens' function-like method (Welter and Rieger, 2010) and

$$c = \int d^3\mathbf{r}' G(||\mathbf{r}' - \mathbf{r}||) \theta\left(o_{TC}^{prol} - o(\mathbf{r}') \right) c(\mathbf{r}') \tag{12}$$

h) The following equation describes the evolution of density field of cancer cells:

$$\frac{\partial b}{\partial t} = -\nabla \cdot J + b^+ + b^- \tag{13}$$

i) where J is the tumor cell flux and b+ and b- are source (cell birth) and sink (cell death) terms, respectively. The flux depends on the gradient of tumor pressure P:

$$P = \begin{cases} \dfrac{b - c_b^{norm}}{c_b^{\max} - c_b^{norm}} & c_b^{norm} \le b \le \\ 0 & b < c_b^{norm} \end{cases} \tag{14}$$

In the model we have introduced an additional flux component equal to $r_b \nabla A$ (Ramis-Conde, et al., 2008), which is responsible for interaction between degraded extracellular matrix and cancer cells. Hence:

$$J = -D_b b(\nabla P + r_b \nabla A) \tag{15}$$

For each of skin layer we have assumed a proper diffusion coefficient D_b of tumor cells by employing experimental data from (Manning, 2013). The diffusion coefficients reflect various proliferation speeds of tumor cells in corresponding skin layers.

j) The sources and sinks are computed from the following expressions:

$$b^+ = \frac{b_1}{T_{TC}^{prol}} \left(1 + \frac{\tau_b A}{\tau_b A + 1} P_b\right) \left(1 - \frac{b}{c_b^{\max}}\right) \quad if \quad o > o_{TC}^{prol} \tag{16}$$

,

$$b^- = -\frac{1}{T_{TC}^{death}} b \quad if \quad o < o_{TC}^{death} \tag{17}$$

k) The next equation represents time evolution of ECM density in tissue:

$$\frac{\partial M}{\partial t} = -\beta_M MB \tag{18}$$

.

l) The evolution of density A of degraded ECM in the tissue is described by:

$$\frac{\partial A}{\partial t} = \gamma_A Mb + \chi_{oA} \Delta A - \gamma_{oA} A \tag{19}$$

.

Hence, vector **x=**(b,n,c,f,m,M,A) is the state vector of all dynamical system variables representing concentration fields in 3-D space. To implement the model in the most efficient way on multiple GPU boards in CUDA environment, we have introduced some simplifications.

First of all, we approximated the formula described by Eq.12, by the Poisson equation, where $c^{(B)}$ means the density of necrotic cells, hence:

$$\Delta c = \alpha_c c^{(B)} \tag{20}$$

.

Similarly, the equation responsible for oxygen distribution was also simplified and reads now:

$$\Delta o = \alpha_o o^{(B)} \tag{21}$$

where α_c and α_o are the constants (see Table 1). It is not necessary to solve this equations in every timestep. We periodically match the concentration density of oxygen to follow the diffusion limits reported in (Manning, 2013). Having in mind that dynamics of vasculature is a key process influencing tumor dynamics, we included to our model the most of processes described in (Welter and Rieger, 2010) such as vessel sprout initiation, sprout migration, vessel wall degradation and their collapse.

In this paper, we consider partially coupled supermodel, i.e., the system of sub-models is linked by a single variable, namely, density of tumor cells $x^1=b$ (see Eq.13). Because we are focused on the growth type dynamics, we decided to construct the supermodel by using three melanoma sub-models differing in values of r_b (see Eq.15) i.e., r_b=0.0001, 0.0003, 0.0005, respectively. Just r_b is directly responsible for the speed of tumor growth. We simulate the spatio-temporal dynamics of uncoupled model consisting of three independent sub-models (i.e., $\mathbf{C}=\{\mathbf{0}\}$ and the supermodel is represented as the average of sub-models (Eq.3)) and three supermodels connected by "weak" $\mathbf{C_w}^1$, "strong" $\mathbf{C_s}^1$ and "very strong" $\mathbf{C_{vs}}^1$ coupling coefficients:

$$\mathbf{C_w}^1 = \begin{matrix} 0.0 & 0.002 & 0.002 \\ -0.002 & 0.0 & 0.002 \\ -0.002 & -0.002 & 0.0 \end{matrix} \quad \mathbf{C_s}^1 = \begin{matrix} 0.0 & 0.25 & 0.125 \\ -0.25 & 0.0 & 0.25 \\ -0.125 & -0.25 & 0.0 \end{matrix} \quad \mathbf{C_{vs}}^1 = \begin{matrix} 0 & 0.5 & 0.25 \\ -0.5 & 0 & 0.5 \\ -0.25 & -0.5 & 0 \end{matrix}$$

We have checked that increasing the number of sub-models l does not change substantially the supermodel behavior. The coupling term between sub-models is turned on after 2500 timesteps to avoid the amplification of large errors produced at the beginning of simulations and caused by different tumor growth speeds for various r_b. The quality of models synchronization is measured by summing the synchronization error from Eq.4 over all sub-models pairs (μ,ν) $(\mu,\nu = 0,1,2)$.

Table. 1 Description of the melanoma model parameters and their values.

Symbol	**Description**	**Value** *(dimless)*
ρ_n	Haptotactic cell migration (Chaplain, et al. 2006)	0.28
D_n	Diffusion of endothelial cells (Chaplain, et al. 2006)	0.0003
χ_n	Chemotactic cell migration (Chaplain, et al. 2006)	0.38
δ_n	Chemotactic constant (Chaplain, et al. 2006)	0.6
η_c	TAF consumption rate (Chaplain, et al. 2006)	0.025
β_f	Production rate of fibronectin (Chaplain, et al. 2006)	0.0125
γ_f	Degradation rate of fibronectin (Chaplain, et al. 2006)	0.1
α_m	Production rate of MDE (Chaplain, et al. 2006)	0.0000015
ε_m	Diffusion coefficient of MDE (Chaplain, et al. 2006)	0.0025
υ_m	Degradation rate of MDE (Chaplain, et al. 2006)	0.75
D_b	Diffusion coefficients of tumor cells in the air and various skin layers (*StratumCorneum, StratumSpinosum, BM, Dermis, Hypodermis*) (Manning, 2013)	20; 83.0; 8.3; 41.5; 20;0.0166
r_b	Tumor cells chemoattractant sensitivity (Manning, 2013)	1-3-5x10^{-4}
c_b^{norm}, c_b^{max}	Normal and maximum density of tumor cells (Welter and Rieger, 2010)	1;2
T_{TC}	Tumor cells proliferation time (Welter and Rieger, 2010)	10
τ_b	Instantaneous reaction rate (Ramis-Conde et al., 2008)	0.5
o_{TC}	Tumor cells proliferation O_2 threshold (Welter and Rieger, 2010)	0.1
P_b	Maximum stimulated mitosis rate (Ramis-Conde et al., 2008)	0.001
T_{TC}^{death}	Hypoxic tumor cells survival time (Welter and Rieger, 2010)	100
o_{TC}^{death}	Tumor cells hypoxia O_2 threshold (Welter and Rieger, 2010)	0.01
γ_A	Production rate of attractants (Ramis-Conde et al., 2008)	0.5
μ_{oA}	Decay rate of the digested ECM (Ramis-Conde et al., 2008)	0.01
$\chi_{\alpha A}$	Diffusion coefficient of the digested (Ramis-Conde et al., 2008)	0.01
α_c	Diffusion rate of TAF(Manning, 2013)	1
α_o	Diffusion rate of O_2 (Manning, 2013)	1
Δt	Timestep (min.)	6
$\lvert\Delta r\rvert$	Mesh size (μm)	20
Nt	Number of timesteps in simulations.	2x10^4

The supermodel equations are discretized on a cubic grid of size 250x250x150, filling the layout from Fig.1. We ran the simulations on a single node of GPGPU server, equipped with one CPU Intel Xeon X5660, 2.8 GHz (6 cores) and 4 Nvidia boards EVGA GeForce GTX 580. As shown in Fig.2a, the computational box is decomposed among 4 GPU boards. In Fig.2b, we present the execution time and

speedups related to 1 CPU and 1 GPU. Unfortunately, in our code the computations spending on vessels remodeling should be executed on CPU. This considerably slows down the computations performed on multiple GPU boards, that is why, the speedup equal to 1.4 on 4 GPUs is not impressing. However, GPU implementation of the code, ensures adequate computational power for our simulations giving in total speedup close to 60 comparing to a single core of Intel Xeon CPU.

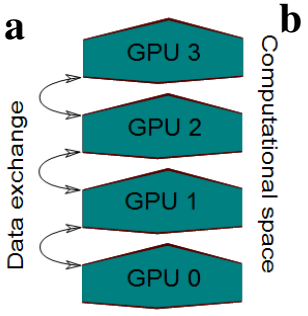

System configuration	Execution time [seconds]	Speed-up to 1 CPU	Speed-up to 1 GPU
Xeon X5660	12720	1	-
1 GTX580	307	41	1
2 GTX580	255	50	1,2
3 GTX580	224	56,7	1,37
4 GTX580	218	58,3	1,41

Figure 2. a) Domain decomposition of the computational box and b) Execution time and speedups obtained for 1000 timesteps.

Results of modeling

As shown in Fig.3a, the sub-models do not synchronize for uncoupled and weakly coupled models. What is rather surprising, the weakly coupled supermodel synchronizes even worse than the uncoupled model. Furthermore, these two models are deficient, producing nonphysical shifts in tumor cell density (see Fig.3b). Conversely, the supermodels with strong and very strong couplings synchronizes very well. The slow growth of synchronization error (see Eq.4) for the strongly coupled supermodel after 8000 timesteps is caused by the fact that the tumor is expanding very fast and reaches the boundaries of the computational box very quickly what introduces additional numerical errors. This effect is negligible small for the very strongly coupled supermodel. As shown in Fig.4, due to small synchronization error, also the standard deviation calculated in every node of computational grid for all sub-models is the smallest for the strongly and very strongly coupled supermodels.

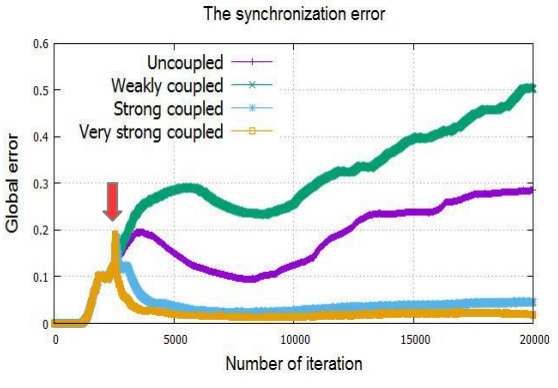

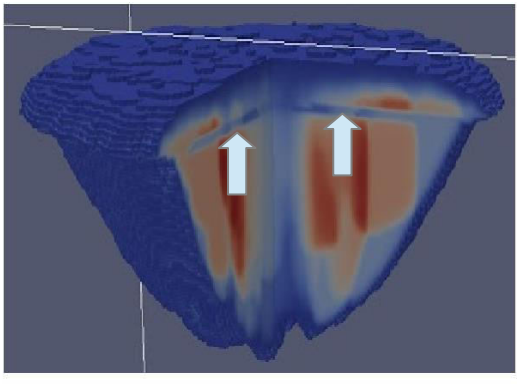

Figure 3: a) The synchronization error (Eq.4) for uncoupled model and weakly, strongly and very strongly coupled supermodels. The red arrow shows the moment of turn on the sub-models coupling (*Nt*=2500 timestep). b) Tumor cell density produces nonphysical shifts (see white arrows) for the first two cases.

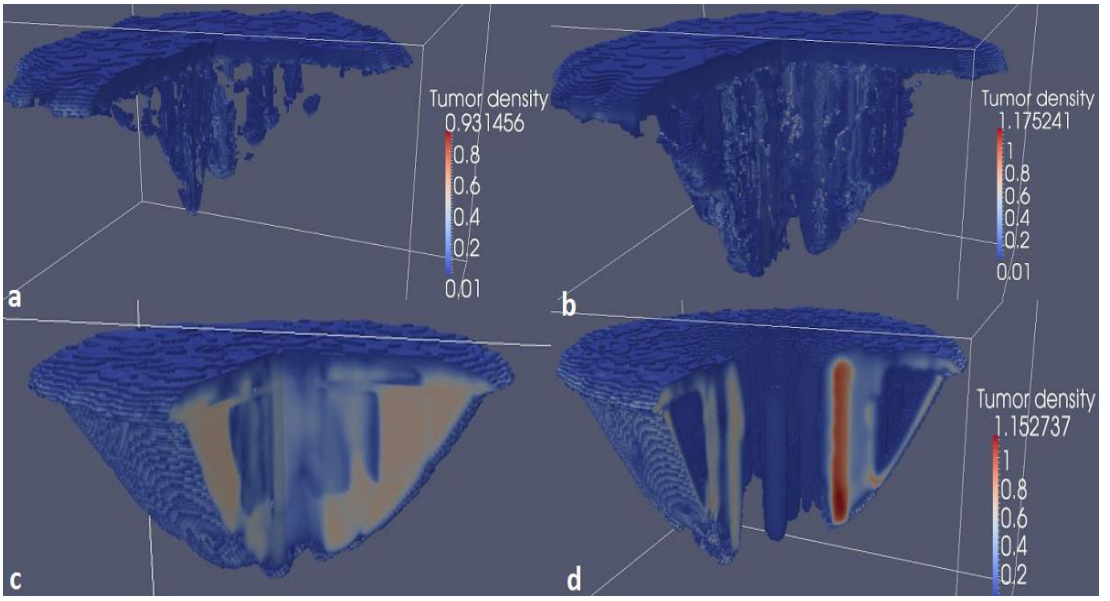

Figure 4: The standard deviations calculated per each computational grid node for the supermodel with a) the strongest coupling strength, b) the supermodel with strong and c) weak couplings. In d) we display the case with the lack of coupling between sub-models. The supermodels (a) and (b) demonstrate very good synchronization between the sub-models. The largest error is colored in rad while the lowest one in blue.

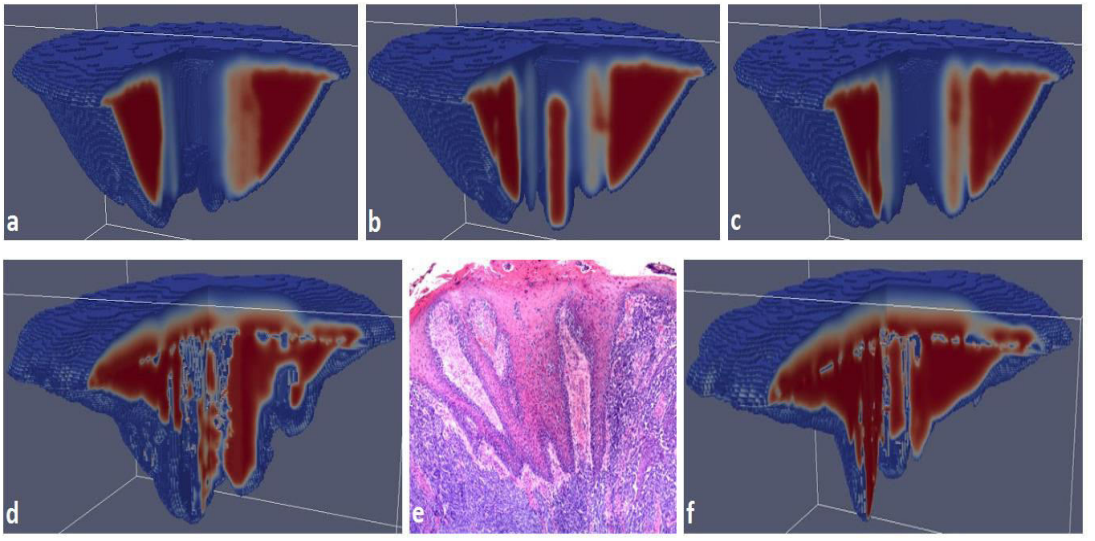

Figure 5: Snapshots from melanoma simulation obtained by: (a,b,c) independent melanoma models for r_b=0.0001, 0.0003, 0.0005 after Nt=1.6-1.4-1.2x10^4 timesteps, respectively; d) the strongly coupled supermodel after Nt=10^4 timesteps; f) the very strongly coupled supermodel after Nt=0.8x10^4 timesteps. The sizes of all tumors are approximately the same. Density of tumor cells is displayed in colors from red (the highest) to blue (the lowest). The necrotic center is invisible. e) The micrograph image of *acral lentiginous* melanoma is included for comparison (www.mmmp.org/MMMP).

In Fig.5(a,b,c) we display the structures of simulated tumor for three melanoma models which differ in value of $r_{b,}$. Greater value of r_b means faster tumor proliferation. The models producing snapshots from Fig.5a,b,c are uncoupled and were run independently. One can recognize growth structures typical for nodular melanoma in which tumor spreads out both radially and vertically from its center, and develops the cone-like shaped nodules.

In Fig.1 and Fig.5d,f we present the snapshots from simulation of melanoma progression produced by very strongly and strongly coupled supermodels, respectively. In Fig.1 one can see the tumor location in skin and its shape after approximately ten weeks of growth. The tumor penetrates *dermis* and proceeds towards *hypodermis*. The real process of melanoma growth is preceded by a long lasting silent phase of tumor cells development, which is neglected in our simulations. However, its growth considerably accelerates in the later phases, so the estimated evolution time is quite realistic.

As shown in Fig.5d, the supermodel demonstrates qualitatively different behavior, which is similar to the *acral lentiginous* melanoma (Fig.5e) with stronger bias to superfacial radial growth. This qualitative difference can also be seen in Fig.6. One can see that for both the strong and very strong supermodel cases, melanoma grows distinctly faster (see the scale of Y axes in Fig.6). Consequently, for the single model with r_b=0.0003 the necrotic center is developed much later than for the supermodel. In Fig.5a,b,c the necrotic centers have not developed after Nt=1.4x10^4. Meanwhile, it is quite large for the strongly and very strongly coupled supermodels after Nt=10^4 timesteps. By further increase of the coupling strength one can obtain the situation from Fig.1, where superficial growth dominate over vertical tumor expansion. This way the various types of simulated melanoma can be potentially obtained by setting different values of coupling factors in the supermodel. It shows the supermodel high flexibility to follow (by minimization of the cost function from Eq.5) the real scenario of melanoma growth, which can be hidden in data.

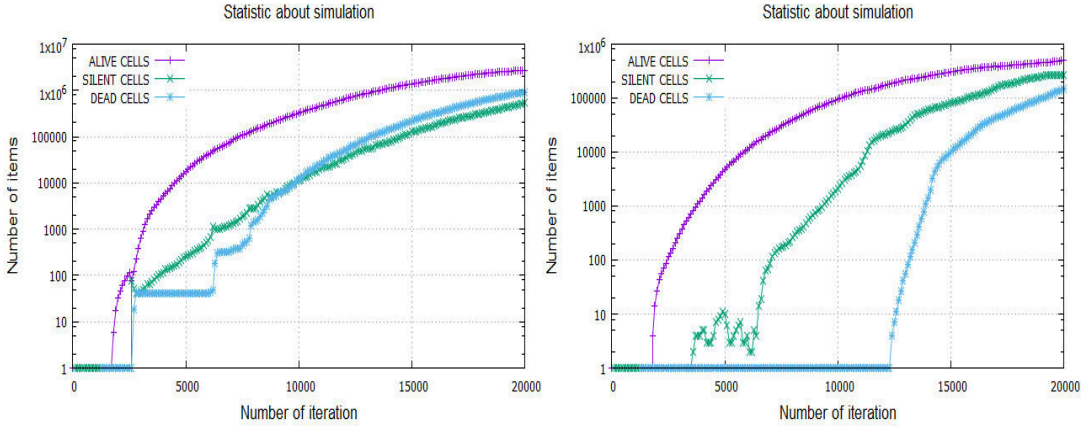

Figure 6: The plots showing tumor growth dynamics – the number of tumor cells with iteration number Nt (time) – for the supermodel from Fig.4d and the single model with r_b=0.0003 (Fig.4b).

Conclusions

It is widely expected (e.g. (Bellomo, et al., 2008; Deisboeck, et al., 2011; Wolkenhauer, et al., 2014)) that planning cancer treatment in oncology of the future will be based on mathematical tumor models. We postulate here that these models could simulate only the key processes influencing tumor dynamics, and should be as simple as possible. The simplified tumor models can be combined to create the supermodel – a flexible coarse-grained modeling framework. All the fine-grained tumor

features and other unpredictable events, accompanying its proliferation and not included in the sub-models, are hidden in data. Just the supermodel coupling coefficients, learned from data according to the prediction/correction scheme – similar to that used in weather forecast and climate modeling – will represent these latent tumor features. In this paper we demonstrate the results, which testify only the first part of this postulate. To this end we have developed the numerical 3-D model of melanoma by assuming the computational layout, which mimics the real structure of skin. Then we have created its supermodel by coupling three sub-models differing in values of a single parameter responsible for tumor growth. We observe that for the uncoupled and weakly coupled sub-models both radial and vertical growth rates are approximately the same. Meanwhile, the strongly and very strongly coupled sub-models synchronize each other and produce qualitatively different scenarios of melanoma growth. For relatively high coupling strength the radial growth of tumor begin to dominate. Depending on the values of the coupling coefficients we have obtained simulation results mimicking recognized melanoma types: nodular (Fig.5a), *lentigo maligna* (Fig.5f), and a*cral lentiginous* melanoma (Fig.5d). The fourth type, i.e., superficial spreading melanoma, we have obtained for even stronger coupling. All of these observations show that the supermodel can be fit to the various scenarios of tumor growth.

The second part of our postulate will be verified in the nearest future in a similar way as it was demonstrated in deliverables of SUMO EU project. First, we plan to check in what extent the PDE based supermodel can predict the behavior of the "ground truth", represented by more advanced model of tumor or a model which exploits completely different computational paradigm (e.g., the PAM particle automata model (Wcisło, et al., 2009; Dzwinel, et al., 2016)). The experiments will be performed for sub-models of various complexity to find the most parsimonious supermodel, which could be a part of a future system for planning cancer treatment. Second, we will try to couple our model with real data coming, e.g., from tumor tomography images.

However, to use our supermodeling scheme for making diagnosis of realistic cancer dynamics it should be enforced by diagnostic methods, e.g., based on *in vivo* nanosensors and new MRI imaging techniques (such as in (Chen, et al., 2015)), which will be developed and widely available in the future. They should allow to measure simultaneously the concentrations of tumor cells and oxygen in many locations distributed in the tumor mass. These measurements could be used directly in the prediction/correction learning scheme of the supermodel coupling coefficients.

Acknowledgements: This research is financed by the Polish National Science Centre (NCN), project DEC2013/10/M/ST6/00531. Thanks are due to Professor Dr Arkadiusz Dudek from University of Illinois Cancer Center for his valuable comments and encouragement.

References

1. Alpaydin, E. (2014). *Introduction to machine learning*. MIT press. pp. 640
2. Barillot, E., Calzone, L., Hupe. P., Vert, J.P. and Zinovyev, A. (2012). *Computational systems biology of cancer*. CRC Press, pp.. 461
3. Bellomo, N., Li, NK., and Maini, PK. (2008). On the foundations of cancer modelling: selected topics, speculations, and perspectives. *Mathematical Models and Methods in Applied Sciences*. 18(04), 593-646
4. Chaplain, M.A., McDougall, S.R. and Anderson, A.R.A. (2006). Mathematical modeling of tumor-induced angiogenesis. *Annu. Rev. Biomed. Eng.* 8, 233-257
5. Chen, L.Q., Randtke, E.A., Jones, K.M., Moon, B.F., Howison, C.M. and Pagel, M.D. (2015). Evaluations of Tumor Acidosis Within In Vivo Tumor Models Using Parametric Maps Generated with AcidoCEST MRI. *Molecular Imaging and Biology*. 1-9
6. Deisboeck, T.S., Stamatakos, GS. (2010). *Multiscale cancer modelling*. CRC Press, pp.484

7. Deisboeck, T.S., Wang, Z., Macklin, P., and Cristini, V. (2011). Multiscale cancer modeling. *Annual review of biomedical engineering*. 13
8. Hinton, G.E., Osindero, S. and Teh, Y.W. (2006). A fast learning algorithm for deep belief nets. *Neural computation.* 18(7), 1527-1554
9. Duane, G.S., Tribbia, J.J. and Weiss, J.B. (2006). Synchronicity in predictive modelling: a new view of data assimilation. *Nonlinear Processes in Geophysics.* 13, 601–612
10. Duane, G.S. (2009). Synchronization of extended systems from internal coherence. *Phys.Rev.E.* 80, 015202
11. Hiemstra, P.H., Fujiwara, N., Selten, F.M., and Kurths, J. (2012). Complete synchronization of chaotic atmospheric models by connecting only a subset of state space. *Nonlinear Processes in Geophysics*. 19(6), 611-621
12. Dzwinel, W., Wcisło, R., Yuen, D.A., Miller, S. (2016). PAM: Particle Automata in modeling of multi-scale biological systems. *ACM Transactions on Modeling and Computer Simulation.* 26(3), A20, 1-21
13. Manning, C.S. (2013). *Heterogeneity in melanoma and the microenvironment.* PhD Thesis, University College London, January 2013
14. Mirchev, M., Duane, G.S., Tang, W.K.S and Kocarev, L. (2012). Improved modeling by coupling imperfect models. *Commun. Nonlinear Sci. Numer. Simul.* 17(7), 2741–2751
15. Ramis-Conde, I., Chaplain, M.A. and Anderson, A.R. (2008). Mathematical modelling of cancer cell invasion of tissue. *Mathematical and Computer Modelling.* 47(5), 533-545
16. van den Berge, L.A., Selten, F.M., Wiegerinck, W. and Duane, G. (2011). A multimodel ensemble method that combines imperfect models through learning. *Earth System Dynamics*, 2(1), 161–177
17. Vittorio, C., Lowengrub, J. (2010). *Multiscale modeling of cancer: an integrated experimental and mathematical modeling approach.* Cambridge University Press, pp.278
18. Welter, M. and Rieger, H. (2010). Physical determinants of vascular network remodeling during tumor growth. *The European Physical Journal E.* 33(2), 149-163
19. Wcisło, R., Dzwinel, W., Yuen, D.A., Dudek, A.Z. (2009). A new model of tumor progression based on the concept of complex automata driven by particle dynamics. *Journal of Molecular Modeling*. 15(12), 1517 –1539
20. Wodarz, D., and Komarova, N.L. (2014). *Dynamics of cancer: mathematical foundations of oncology*. World Scientific, pp.514
21. Wolkenhauer, O., Auffray, C., Brass, O., Clairambault, J., Deutsch, A., Drasdo, D., Gervasio, F., Preziosi, L.,Maini, P., Marciniak-Czochra, A., Kossow, C., Kuepfer, L., Rateitschak,K., Ramis-Conde, I., Ribba,B., Schuppert, A., Smallwood, R., Stamatakos, G., Winter, F., Byrne, H. (2014). Enabling multiscale modeling in systems medicine. *Genome Med.* 6(3), 21
22. Yang, S-C., Baker, D, Li, H., Cordes, K., Huff, M., Nagpal, G., Okereke, E., Villafane, J., Kalnay, E. and Duane, G.S. (2006). Data Assimilation as Synchronization of Truth and Model: Experiments with the Three-Variable Lorenz System. *J. Atmos. Sci.* 63, 2340–2354